Rec'd with letter dtd 9/28/97

CRITIQUE OF DOE's NEAR-FIELD ENVIRONMENT MODELING FOR THE PROPOSED HIGH-LEVEL NUCLEAR WASTE REPOSITORY AT YUCCA MOUNTAIN, NEVADA

Prepared for

Nuclear Regulatory Commission
Contract NRC-02-93-005

Prepared by

Peter C. Lichtner
David R. Turner

Center for Nuclear Waste Regulatory Analyses
San Antonio, Texas

February 1997

ABSTRACT

Model calculations are presented for the evolution of the near-field environment for the proposed high-level nuclear waste disposal facility located in unsaturated rock at Yucca Mountain (YM), Nevada. The purpose of this report is to evaluate different approaches which are currently being used to described the near-field environment of the proposed repository. Pure evaporation, solubility limits, and estimates based on MULTIFLO calculations are compared and evaluated. A brief review is given of DOE modeling efforts of the near-field environment based on the recent report by Wilder (1996). An evaluation is presented of the mineralogy at YM which could influence the near-field environment.

CONTENTS

FIGURES

TABLES

ACKNOWLEDGMENTS

This report was prepared to document work performed by the Center for Nuclear Waste Regulatory Analyses (CNWRA) for the Nuclear Regulatory Commission (NRC) under Contract No. NRC-02-93-005. The activities reported here were performed on behalf of the NRC Office of Nuclear Material Safety and Safeguards (NMSS), Division of Waste Management (DWM). The report is an independent product of the CNWRA and does not necessarily reflect the views or regulatory position of the NRC.

We would like to thank Gustavo Cragnolino and Wesley Patrick for comprehensive reviews and Arturo Ramos for formatting the final manuscript.

QUALITY OF DATA, ANALYSES, AND CODE DEVELOPMENT

DATA: CNWRA-generated original data contained in this report meets quality assurance requirements described in the CNWRA Quality Assurance Manual. Sources for other data should be consulted for determining the level of quality for those data.

ANALYSES AND CODES:
The MULTIFLO computer code was used for analyses contained in this report. This computer code is in the process of being controlled under the CNWRA Software Configuration Procedures.

1 INTRODUCTION

The proposed site for disposal of high-level nuclear waste (HLW) at Yucca Mountain (YM), Nevada, is unique in that the site lies above the water table. This circumstance has profound consequences on the behavior of the near-field environment surrounding the repository in response to heat generated by the radioactive waste. Perturbations to the near-field environment caused by emplacement of the waste consist primarily of: (i) changes in aqueous and gaseous phase compositions; and (ii) alteration of the host rock resulting in changes in porosity, permeability, tortuosity, and sorptive properties. Important aqueous and gaseous solution variables that influence degradation of the waste package and spent fuel, and radionuclide transport include the pH, chloride concentration, and oxygen and carbon dioxide fugacities. Alteration of cristobalite to quartz may be an important reaction to consider for the proposed HLW repository at YM, because it could result in a significant increase in porosity and permeability in the near field.

Until recently (Robinson, 1994; White, 1995; Lichtner, 1996; Lichtner and Seth, 1996a) there have been few attempts to couple thermal, hydrologic and chemical (THC) processes to describe quantitatively the evolution of the near-field environment resulting from emplacement of HLW in an unsaturated host rock. A number of authors have presented coupled thermal-hydrologic (TH) model calculations of the redistribution of moisture resulting from emplacement of HLW at the proposed YM repository site (Buscheck and Nitao, 1993; Pruess and Tsang, 1994; Lichtner and Walton, 1994). These calculations are based on two-phase flow codes such as TOUGH (Pruess, 1991), FEHMN (Zyvoloski et al., 1992), and NUFT (Nitao, 1996). Calculations indicate that heat released from the waste as it decays over time, creates a zone of reduced saturation surrounding the repository with enhanced zones of saturation above and below the repository horizon caused by condensation of water vapor. The degree of dryness and time to rewet the repository depend on the heat load of the repository and the hydraulic properties associated with the host rock. At sufficiently high heat loads, heat-pipe effects may occur which are characterized by counter flow of liquid and vapor. Within the heat-pipe region, liquid water flows towards the repository, primarily due to capillary suction, balanced approximately by counter flow of vapor. Gravity has a minimal effect on the dynamics of the heat pipe, as manifested in the asymmetry between heat-pipes formed above and below the repository horizon. Heat pipes are not stationary, but move upward and downward from the repository horizon with time. Eventually, as the heat produced by the waste drops to a sufficiently low level, the heat pipes collapse and the rewetting phase begins.

A possible result of the formation of heat pipes, and associated continual evaporation and refluxing of liquid water lasting for periods of hundreds to thousands of years, is increased salinity in the near-field region and formation of salt precipitates (Murphy and Pabalan, 1994; Lichtner and Seth, 1996a; Walton, 1993). The amount of water that can be evaporated depends not only on the heat loading of the repository, but also on the initial saturation of the pore spaces in the rock adjacent to the waste packages, and on the flow of liquid water towards the waste packages resulting from capillary forces and gravity driven flow including infiltration. Lichtner and Seth (1996a) carried out fully coupled THC calculations using a repository-scale model and demonstrated that even with moderate heat loads substantial increases in salinity and pH, the latter caused by degassing of CO_2, could occur.

The purpose of this report is to evaluate DOE's efforts to date in predicting possible changes in the near-field environment of the proposed high-level nuclear waste disposal facility at YM. Emphasis is placed on estimating changes in aqueous and gaseous phase compositions and mineral alteration, with consequent changes in porosity and permeability. For this purpose, the recently released document: The Near-Field and Altered Zone Environment Report (Wilder, 1996), has served as the basis for the evaluation presented here.

2 DOE NEAR-FIELD AND ALTERED-ZONE ENVIRONMENT REPORT

This report focuses on model calculations of near-field chemistry evolution and chemical alteration of the host rock as a result of emplacement of heat-generating radioactive waste. Sections 3.4.1 and 10.4.4 in Volume II of the recent report issued by DOE (Wilder, 1996) are reviewed. Section 3.4.1 of the DOE report presents results of near-field geochemical modeling based on the computer code EQ6 (Wolery, 1992). In section 10.4.4, results of reactive flow and transport calculations are presented describing alteration of the YM tuff host rock and consequent changes in porosity.

2.1 Evaporation Effects

In section 3.4.1 of the DOE report authored by Glassley (1996), the effects of evaporation of water on aqueous and gaseous phase compositions are modeled using the computer code EQ6. A number of plots are presented showing the concentrations of various species as functions of the number of moles of water evaporated from a beaker initially filled with 1 kg water with the composition of J-13 well water. Several different cases are considered: with and without buffering gas phase fugacities O_2 and CO_2, and with and without precipitation of quartz, tridymite and talc. The choice of these particular mineral phases is not explained. Significant differences are reported for the evolution of pH, and concentrations of Ca^{2+} and SiO_2 depending on the assumptions made for the gas phase composition. Buffering the system at atmospheric CO_2 fugacities leads to an increase in pH as the number of moles of water evaporated increases. In the absence of CO_2 buffering, the pH decreases with increasing evaporation. For nonvolatile species such as chloride, there is no effect on the CO_2 concentration as would be expected, at least at moderate ionic strengths.

There are several shortcomings of the DOE analysis which limit its usefulness for direct application to the proposed YM HLW repository:

- In order to actually apply these results to the repository situation and provide an estimate of the solution composition in the near field, a further step is necessary which is not presented in the DOE report (Glassley, 1996). This step requires relating the number of moles of water evaporated in the EQ6 calculation to the number of moles of water evaporated at a particular point of interest within the near-field region of the repository. This is not done in the report although information is readily available from TH calculations in the form of the liquid saturation, from which the number of moles of water evaporated can be computed.

- Furthermore, the EQ6 calculations presented in the report do not apply to the situation following rewetting after all of the water has been evaporated from the near-field region of the repository. This is an important case related to DOE's extended dry concept. Although the EQ6 calculations could possibly predict which salts precipitate and their amounts upon complete dryout, no results are presented predicting solute concentrations after the rewetting fluid has dissolved the salts. In fact, which salts actually form as complete evaporation is achieved in the high heat load case may be of little importance. This is because of the extremely small amount of salt which will form and because the salts will most likely dissolve immediately upon contact with a thin film of water as rewetting commences.

- Finally, because no connection is made to the actual TH regime established in the repository, *ad hoc* assumptions are necessary which prove critical to predicting the evolution of the aqueous and gaseous phase compositions with time.

2.1.1 Bounding Calculations

To derive bounds on some quantity it must first be determined how tight the bounds need to be, to be useful. Reasonable bounds are usually much more difficult to obtain than absolute bounds, which are often overly conservative to be of much use. In the analysis that follows, three different approaches are compared: pure evaporation in which solute flux is assumed to be negligible; solubility limits derived from saturation with a highly soluble salt such as halite; and finally MULTIFLO calculations which include evaporation, boiling and reflux of liquid water in a fully coupled approach.

2.1.1.1 Pure Evaporation

The increase in solute concentration due to evaporation of water for a nonvolatile and nonreactive species such as chloride, assuming the aqueous solution remains undersaturated with respect to chloride-bearing minerals such as halite, can be easily calculated from the equation

$$m_i = \frac{n_i^0}{M_w^0 - n_w W_w}, \tag{2-1}$$

where m_i refers to the molality of the species in question, n_i^0 denotes the initial number of moles of that species in a given mass of water $M_w^0 = n_w^0 W_w$, n_w represents the number of moles of water evaporated, and W_w = 0.018 kg/mole-H_2O is the molecular weight of water. There are 55.51 moles of water in 1 kg. This relation is valid for a system that is closed with respect to the flux of liquid water into or out of the system. In particular, this same assumption applies to EQ6-type calculations. Shown in figure 2-1 is a plot of Eq. (2-1) for an initial mass of 1 kg water and an initial chloride concentration of 8 mg/kg-H_2O [compare with figure 3.4-6 in Glassley (1996) computed using EQ6 which shows identical results].

To relate Eq.(2-1) to the change in solute concentration in the near-field region of the repository, it is necessary to relate the number of moles of liquid water evaporated to the local value of the liquid saturation of the host rock. Provided the change in liquid saturation is caused by evaporation only, and not by the flux of liquid into or out of the control volume, liquid saturation s_l is related to the number of moles of water evaporated according to the equation

$$1 - \frac{s_l}{s_l^0} = \frac{n_w}{n_w^0}, \tag{2-2}$$

where the quantity n_w^0 represents the initial moles of water in a given volume of bulk rock, and s_l^0 refers to the initial liquid saturation. To obtain this equation note that liquid saturation is defined as the ratio of volume of liquid V_w to pore volume V_p

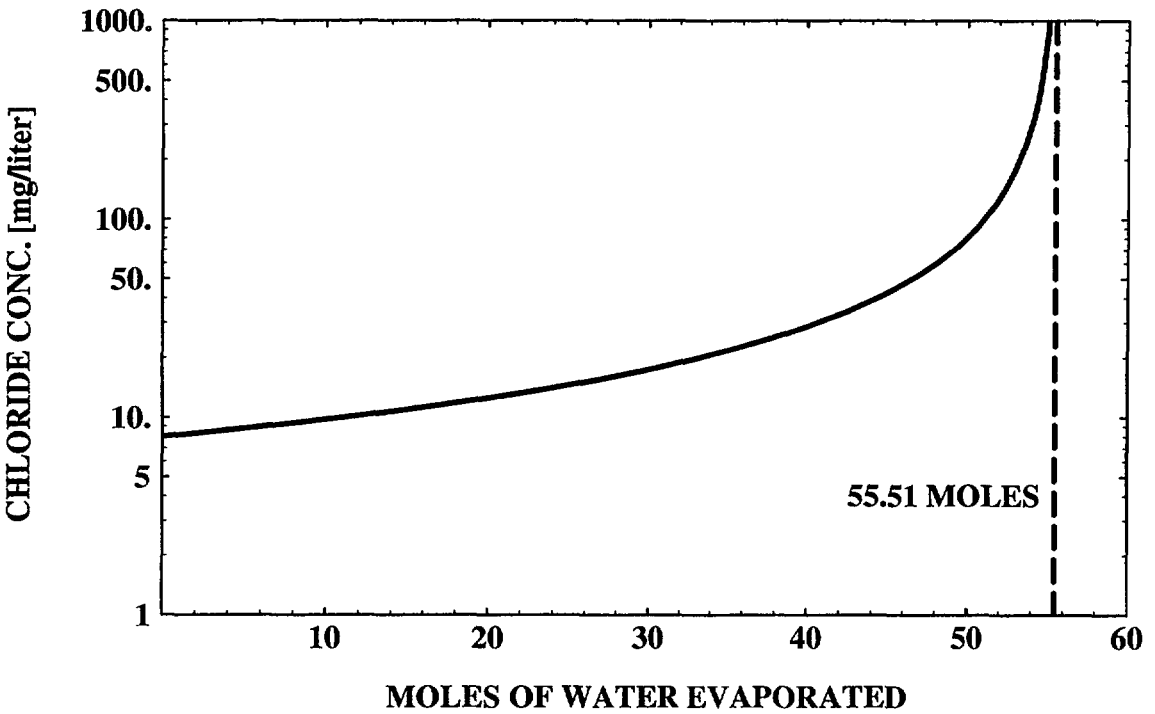

Figure 2-1. Increase in chloride concentration as water is evaporated from a beaker initially filled with 1 kg of water as described by Eq. 2-1. To convert to molality note that 1,000 mg/liter chloride is equivalent to 0.0282 molal at 100°C.

$$s_l = \frac{V_w}{V_p}, \tag{2-3}$$

and the liquid volume is related to the number of moles of water evaporated by the expression

$$V_w = \left(n_w^0 - n_w\right)\bar{V}_w, \tag{2-4}$$

with the initial volume of liquid given by $V_w^0 = n_w^0 \ \bar{V}_w$, and where $\bar{V}_w$ denotes the molar volume of pure water. It follows that the molality is inversely proportional to the liquid saturation

$$m_i = M_i^0 \frac{s_l^0}{s_l}. \tag{2-5}$$

It is useful to define an enrichment factor η_i as the ratio of the concentration of some solute species at time t and location r, to the initial concentration at the same location. For a simple evaporative process, η_i is equal to the ratio of the initial saturation to the actual saturation

$$\eta_i = \frac{m_i}{M_i^0} = \frac{s_l^0}{s_l} = \frac{n_w^0}{n_w^0 - n_w}. \tag{2-6}$$

According to this relation, the enrichment of some solute species due to pure evaporation is inversely proportional to the amount of water remaining in the control volume. If 90 percent of the water is evaporated, the enrichment factor for chloride is approximately 10 (figure 2-1). As complete evaporation is achieved, the enrichment factor tends towards infinity. Clearly, at some point along the evaporation path when the aqueous solution reaches saturation with solid phases (salts), this relation must break down and the concentration becomes solubility limited.

2.1.1.2 Solubility

A solubility-based estimate for the increase in chloride concentration resulting from evaporation may be derived by assuming the aqueous solution comes to equilibrium with a salt (e.g., halite). As evaporation proceeds, it is assumed that the sodium and chloride concentrations remain proportional to one another

$$a_{Na^+} = \alpha a_{Cl^-}, \tag{2-7}$$

with proportionality constant $\alpha \approx 10$, as derived from J-13 well water (see table 2-1). This relationship is correct only if reaction with the solid phase does not remove sodium from solution. Equilibrium with halite implies the mass action equation

$$K = a_{Na^+} a_{Cl^-} = \alpha a_{Cl^-}^2. \tag{2-8}$$

Therefore

$$a_{Cl^-} = \sqrt{\frac{K}{\alpha}}. \tag{2-9}$$

The log K for halite at 100°C is equal to 1.578, according to the EQ3/6 database (Wolery, 1992). (Note that because of vapor pressure lowering caused by capillary forces, the boiling point of water can be raised significantly above 96°C corresponding to the elevation of YM.) It follows that at this temperature the equilibrium activities for chloride and sodium are equal to $a_{Cl-} = 1.945$ and $a_{Na+} = 19.45$. To obtain the actual concentrations, activity coefficient corrections must be applied which could be substantial at these relatively large concentrations.

Table 2-1. Initial fluid composition for major species corresponding to J-13 well water (Harrar et al., 1990)

Species	Molality×10^4
Ca^{2+}	2.90–3.70
Na^+	18.30–21.70
K^+	1.00–1.40
HCO_3^-	1.93–2.34
SiO_2(aq)	95.00–11.40
Cl^-	1.78–2.37
pH	6.8–8.3

$$\eta_{Cl^-} = \frac{C_{Cl^-}}{C^0_{Cl^-}} = \frac{1}{a^0_{Cl^-}}\sqrt{\frac{K}{\alpha}} \sim 10^4. \qquad (2\text{-}10)$$

The chloride concentration in equilibrium with halite could be substantially increased if the sodium concentration is lowered by precipitation of other sodium-bearing solids such as feldspars. Thus this estimate could underestimate the chloride concentration. However, if halite saturation is never reached, the predicted enrichment factor could be orders of magnitude larger than that which actually occurs in the repository. Equal concentrations of sodium and chloride in equilibrium with halite at 100°C implies roughly 6 M concentration of each species. Clearly, it is difficult to find a bound within reasonable limits even for a nonvolatile species such as chloride.

An estimate of the pH is more difficult to obtain and may depend on reactions with the host rock minerals as well as properties of the gas phase. Likewise, calcium and carbonate have no obvious bounds since their concentrations will be pH-dependent and will depend on reaction with calcite, for example.

2.1.1.3 Estimate Based on MULTIFLO Calculations

The computer code MULTIFLO (Lichtner, 1996; Lichtner and Seth, 1996b; Seth and Lichtner, 1996) provides a fully coupled, quantitative description of two-phase fluid flow and reactive transport of aqueous and gaseous species. Heat flow is also accounted for in the code. MULTIFLO simulates the same complexity in chemistry as EQ6. The thermodynamic databases used by the two codes are equivalent.

Fully coupled calculations using MULTIFLO are presented for the change in chloride concentration based on a repository-scale model. The repository is represented as a circular disk with a heat load of 83.4 MTU/acre. For this case, complete dryout does not occur. An initial saturation of

approximately 80 percent throughout most of the unsaturated zone, becoming fully saturated at the water table, is assumed. The initial temperature varies from 15°C at the surface to 30°C at the water table. A single vertical spatial dimension through the center of the repository is considered (see figure 2-2). The repository horizon is located at a depth of 375 m from the surface. Material properties used in the MULTIFLO calculations are listed in table 2-2. Twenty six year old spent fuel is used with a mix of 65 percent PWR and 35 percent BWR.

Table 2-2. Material properties for van Genuchten parameters α, λ, and residual saturation s_r, permeability k, and porosity ϕ used in the MULTIFLO calculations.

Property	Matrix	Fracture	Equivalent Continuum Model
α [m^{-1}]	$5.8\ 10^{-7}$	$1.305\ 10^{-5}$	–
λ	0.44	0.7636	–
s_r	0.08	0.04	–
$k[m^2]$	$1.9\ 10^{-18}$	$3.9\ 10^{-12}$	$7.0219\ 10^{-15}$
ϕ	0.11	0.0018	0.1116

The enrichment factor for chloride predicted by MULTIFLO is compared to the ratio of the initial liquid saturation to the liquid saturation at the same time and location, as given in Eq. (2-6). The latter corresponds to the enrichment that would be obtained if only pure evaporation is taken into account, equivalent to results obtained using the computer code EQ6. Two different residual saturations s_l^r of 0.08 and 0.01 are considered. The residual saturation occurs as a parameter in the van Genuchten relations for saturation and relative permeability in terms of capillary suction (van Genuchten, 1980). Physically the residual saturation, also referred to as the irreducible or equilibrium saturation, represents the threshold liquid saturation at which the liquid phase becomes disconnected, breaking up into isolated islands of liquid water. At and below the residual saturation, the liquid relative permeability becomes zero and flow is not possible. The liquid saturation may be reduced below the residual value by evaporation with water carried away in the vapor phase.

In figure 2-3 the enrichment factor for chloride is displayed as a function of depth for an elapsed time of 100 y, and in figure 2-4 as a function of time at the repository horizon. Three cases are examined. The base case (red curves) corresponds to the parameters listed in table 2-2. The green curves correspond to a residual saturation of $S_l^r = 0.001$, and the blue curves to a residual saturation of $S_l^r = 0.001$ and a fracture permeability of 10^{-11} m^2. The solid curves correspond to the MULTIFLO calculations, and the dotted curves to the pure evaporative estimate. Increasing the fracture permeability or reducing the residual saturation leads to an increase in the chloride enrichment factor. As can be seen from the figures, the pure evaporative enrichment factor closely matches the MULTIFLO calculated value. In the regions of condensation above and below the repository where the aqueous solution becomes more dilute, the pure evaporation enrichment factor exceeds the MULTIFLO calculated value. This difference in behavior can be attributed to dilution of the total inventory by the flux of condensate fluid. This factor is not accounted for in the pure evaporation calculation. At early times, the flux adds solute species to the control volume, whereas at later times, because the refluxing fluid is more dilute than the ambient groundwater concentration, a reduction in the enrichment factor ensues.

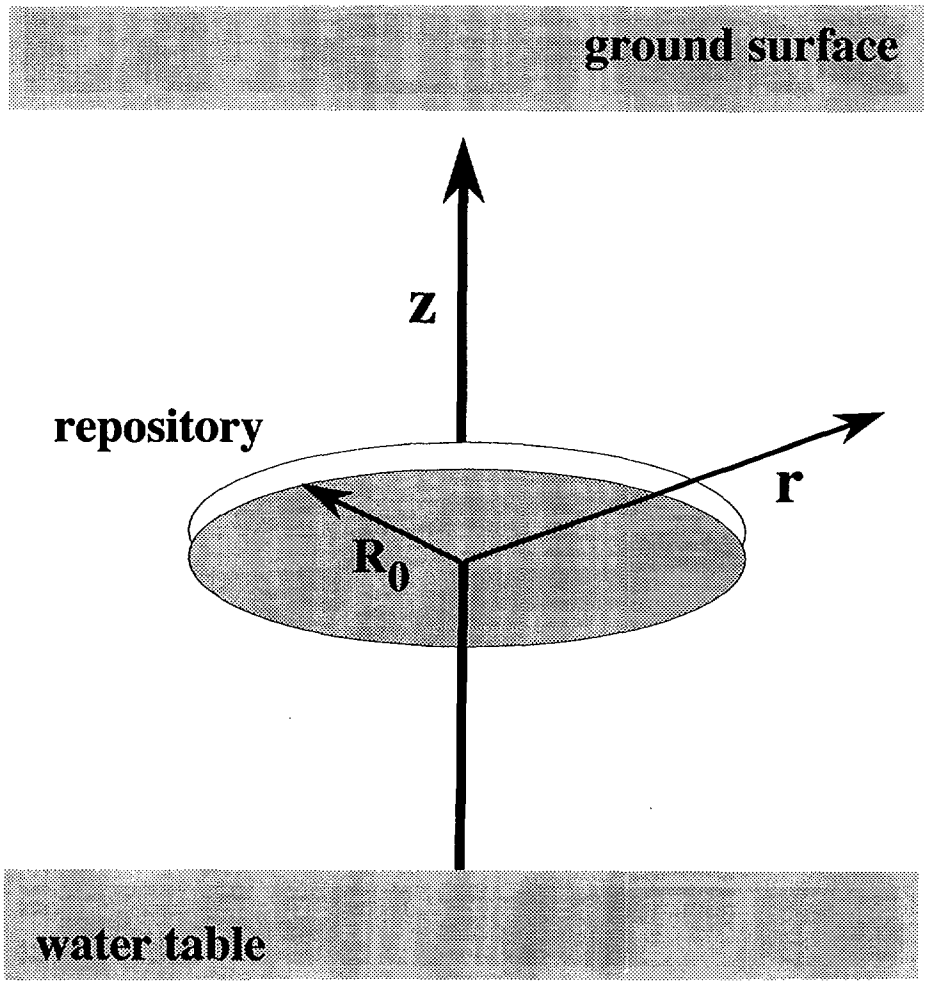

Figure 2-2. Repository-scale model

It is apparent that pure evaporation calculations alone are insufficient and relatively limited in their ability to bound the aqueous and gaseous phase compositions that would result from extended boiling and evaporation of liquid water in the near-field region of the repository. Mechanisms responsible for determining how the solute concentration changes with changing temperature and moisture content include both boiling and evaporative effects and reflux of liquid water including infiltration. There are two cases to consider: the first case corresponds to a heat load for which complete dryout does not occur; and the second case to a heat load for which complete dryout does occur. In the first case, the enrichment factor for a nonreactive species such as chloride is roughly equal to the amount of water evaporated. Saturation of chloride with halite or other chloride-bearing minerals is presumed not to occur and, therefore, in this case a simple evaporation model may be used. What is needed is a TH calculation providing the liquid saturation, which determines the amount of water evaporated. As evaporation proceeds, the liquid saturation will eventually fall below the residual saturation for the medium assuming there is sufficient heat supplied by the spent nuclear fuel and infiltration is sufficiently low. For saturations at or below the residual saturation, the aqueous phase consists of isolated islands of liquid and as a result the liquid flux becomes vanishingly small because of the small liquid relative permeability. Thus, under these

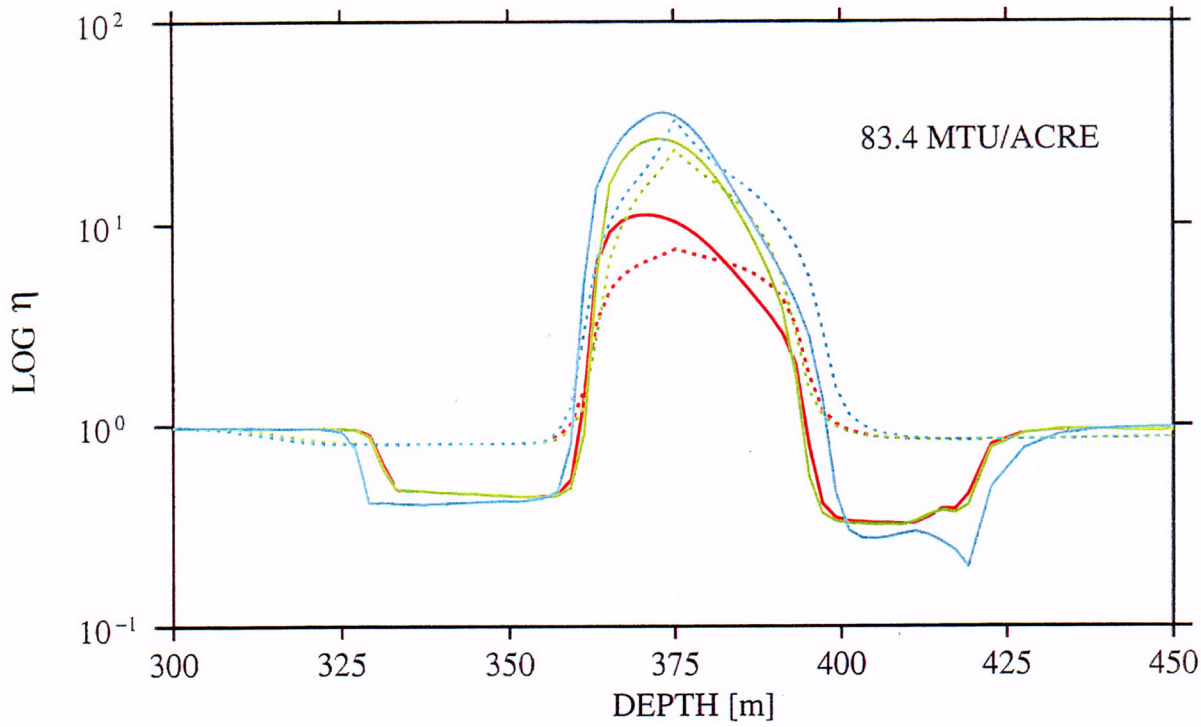

Figure 2-3. Enrichment factor for chloride at 100 y plotted as a function of depth computed using MULTIFLO compared with the simple evaporation model. See text for explanation.

circumstances, regions of extreme dryout which are below the residual saturation act as closed systems with respect to flow of liquid. The vapor phase, however, is free to move throughout these regions.

The second case, however, is more complicated. In this case, all dissolved species precipitate out as salts during complete dryout, and then redissolve as the rewetting phase takes place. Therefore, the solution concentration is determined by the amount of water present during the rewetting phase—not on the amount of water evaporated. Thus it is the rate of reflux of water, including the contribution from infiltration at the surface, into the dryout zone which is most important. This quantity lies outside the scope of EQ6 calculations. Because the rate of rewetting proceeds much more slowly compared to dryout, much larger concentrations can be expected during the rewetting phase. For this case, EQ6-type calculations which consider evaporation only and predict the stable mineral assemblage at complete dryout,

C-01

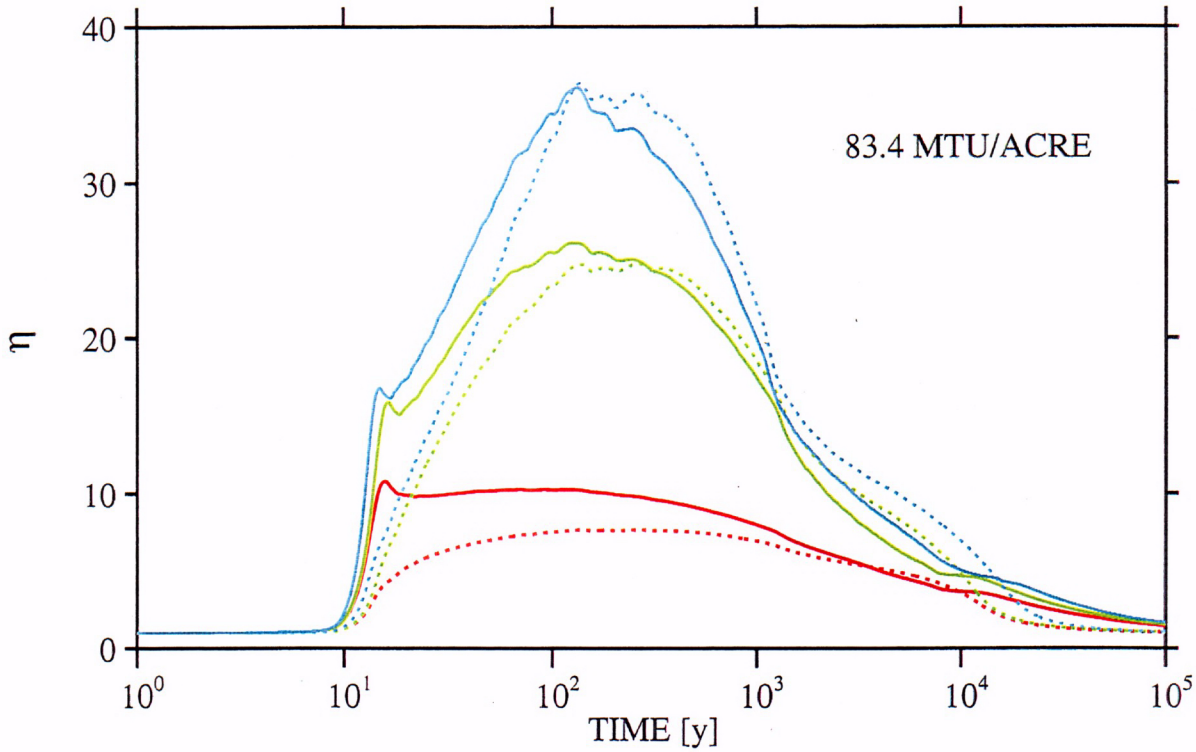

Figure 2-4. Enrichment factor for chloride at the repository horizon plotted as a function of time at the repository horizon computed using MULTIFLO compared with simple evaporation model. See text for explanation.

provide *no* information whatsoever regarding the solution composition during the rewetting phase. Knowing the extent of resaturation, it may be possible to run EQ6 calculations in reverse and obtain the solution composition resulting from adding liquid water to the mineral precipitate obtained during dryout. However, this has not yet been done to the authors' knowledge. In essence, this is what the computer code MULTIFLO accomplishes by combining a reactive transport calculation with a thermal-hydrologic calculation to determine the temperature, liquid saturation, aqueous and gaseous compositions, and mineral deposition profiles with time. Such calculations are currently in progress for the complete dryout case.

C-02

2.2 ALTERED ZONE

In section 10.4.4, Formation of Flow and Transport Barriers Within The Altered Zone, by Johnson and Glassley (1996), calculations are presented describing alteration of YM tuff using the code GIMRT (Steefel and Yabusaki, 1995). This code applies to fully saturated conditions only, and does not include transport of gaseous species. As such, GIMRT is not able to describe the distribution in temperature, pressure, and moisture content resulting from emplacement of nuclear waste in the unsaturated zone. The code GIMRT is similar to the code GEM (Lichtner and Seth, 1996b) when used in a fully saturated mode and provides similar functionality. In particular, GIMRT uses the same database as GEM, which was derived from the EQ3/6 database (Wolery, 1992).

Input data to the calculations require specifying: (i) initial and boundary fluid compositions, (ii) initial composition of host rock in terms of mineral volume fractions, (iii) porosity, (iv) possible secondary alteration products, (v) flow velocity (constant), (vi) temperature profile (constant), and (vii) kinetic rate constants and surface areas of all reacting minerals.

Three separate applications are considered in this section. The first is a benchmark simulation carried out at 238°C. The computer code GIMRT is compared with experimental data. The remaining applications describe alteration of backfill material and the YM host rock. The second application describes alteration of backfill at 250°C for six months and at 90°C with a continuous fluid flow rate of 266.7 m/y. Johnson and Glassley (1996) do not question whether liquid water would in fact be present at temperatures as high as 250°C in the repository environment which seems highly unlikely. The third application describes alteration of the host rock. Johnson and Glassley (1996) considered a fully saturated system with a Darcy flow rate of 2.67 m/y maintained over a period of 10,000 y. A 10 m one-dimensional (1D) flow column is considered with a constant temperature of 95°C over the first 5 m, and a temperature gradient of 1°C/m over the second 5 m of the column. The flow velocity is orders of magnitude larger than the liquid velocity computed for a repository thermal loading of 83.4 MTU/acre, for example. Furthermore, it is difficult to understand how a flow rate of this magnitude could be maintained for a period of 10,000 y. No mention is made, however, of the thermal loading assumed for the repository. Reference is made to the extremely low, fracture-controlled permeability quoted as 10^{-18} m^2. In fact, this value corresponds to the matrix permeability (Lichtner and Walton, 1994). The combined fracture-matrix permeability is much higher than this as derived from the equivalent continuum model (Lichtner and Walton, 1994).

An extremely dilute solution is used for the infiltrating fluid. Because the infiltrating fluid is supposed to result from the condensate zone it is argued that its composition should approach distilled water. However, this neglects mixing of the condensate fluid with the ambient groundwater. Very likely the fluid composition in the condensate zone is only slightly more dilute than the ambient groundwater as a result of mixing.

Primary minerals used to represent the host rock are presented in table 2-3 along with their initial concentrations. Associated kinetic rate parameters are listed in table 2-4. Dissolution times are calculated from Eq.(A-15) given in the Appendix. The use of endmember stoichiometric phases such as anorthite, k-feldspar and albite is questionable as these phases have not been identified in the YM host rock. Also somewhat questionable in the calculation appears to be an indiscriminate use of secondary minerals. Pyrophyllite, for example, is used as a secondary mineral. This mineral, however, usually forms only at much higher temperatures than occur in the simulation.

Table 2-3. Primary mineral concentrations used by Johnson and Glassley (1996)

Mineral	Volume fraction	Weight percent
cristobalite	0.3960	0.413
quartz	0.1341	0.159
k-feldspar	0.2042	0.233
albite	0.1507	0.176
anorthite	0.0050	0.006
porosity	0.11	—

Several difficulties emerge from this analysis based on a simplified picture of the flow geometry:

- Because it was not possible in the model calculations to include the actual TH flow regime, it was necessary to make *ad hoc* assumptions which did not adequately represent the situation expected at the repository.
- The initial fluid composition could not be adequately determined and as a result an extremely dilute solution was used to represent the condensate, but which did not take into account mixing with the ambient groundwater.
- The temperature profile and its variation with time could only be guessed at and may not adequately describe the actual repository setting. The temperature is crucial in determining mineral reaction rates and conditions necessary for moisture to be present.
- Johnson and Glassley (1996) give no justification for the values of the reaction rates they used in their calculation of the altered zone. The reactive surface areas of primary minerals are perhaps the most crucial data needed to obtain meaningful results.

2.2.1 Mineralogy of Yucca Mountain

The mineral composition and associated grain size distribution is highly variable at YM, both vertically and laterally. One can imagine that variations in mineral composition and surface areas could lead to different rates of alteration and hence variations in solution composition, secondary porosity and permeability. Such effects, in turn, could alter the redistribution of moisture as a consequence of emplacement of the repository and its perturbation in the ambient temperature. As a result it is difficult, and may not be conservative to choose a representative composition for the whole mountain.

Mineralogy and mineral abundances for hydrostratigraphic units at YM have been determined using quantitative X-ray diffraction (XRD) and summarized in the synthesis report on mineralogy and petrology studies (Vaniman et al., 1996). Mineralogy has been determined for cores taken from 21

Table 2-4. Rate constants for primary minerals used by Johnson and Glassley (1996) and derived surface areas, grain sizes, and dissolution times for an initial volume fraction of 10 percent

Mineral	Effective rate constant		Rate constant 25°C	Surface area	Grain size	Diss. time
	[vol.%y^{-1}]	[moles cm^{-3} s^{-1}]	[moles cm^{-2} s^{-1}]	[cm^{-1}]	[cm]	[y]
cristobalite	0.1	−12.38	−16.34	23.5	0.1	1,188
quartz	0.01	−12.85	−17.39	88.19	0.01	4,230
k-feldspar	0.001	−14.54	−16.50	5.09	0.24	61,260
albite	0.1	−12.50	−16.26	318.1	0.0028	452.1
anorthite	0.001	−14.50	−12.55	0.0006	48.6	1,500

different wells drilled in the vicinity of YM. Figure 2-5 summarizes the mineral abundances in drill holes USW G-4 and UE-25 UZ #16. Only the location of the Topopah Spring Tuff is shown for clarity. Table 2-5 summarizes the depth to the water table and the thicknesses of the different hydrostratigraphic units.

In both USW G-4 and UE-25 UZ #16, the top volcanic unit is the Tiva Canyon Tuff. Mineralogy in the Tiva Canyon is dominantly cristobalite and alkali feldspar. A thin basal vitrophyre is dominated by glass, with minor feldspar and cristobalite. Beneath the Tiva Canyon lie the YM and Pah Canyon Tuffs (USW G-4) and Paintbrush bedded tuff (UE-25 UZ #16). These tuffs are dominantly glass, feldspar, and smectite. Thin layers rich in clay and smectite have apparently formed at the expense of feldspar and/or glass immediately above and within the vitrophyres, suggesting perhaps that focused flow along the vitrophyre interface has led to increased alteration.

Within the repository block, the Topopah Spring Tuff is about 300–350 m thick. Mineralogy is dominated by alkali feldspar (overall average composition of $Or_{0.50}Ab_{0.42}An_{0.08}$, Or-orthoclase, Ab-albite, An-anorthite) and silica polymorphs (tridymite, α-cristobalite, quartz). Based on mineral abundances, the Topopah Spring Tuff can be broadly divided into four units. At the top lies a vitrophyre unit that is almost entirely composed of glass. Beneath the vitrophyre, the tuff is devitrified with alkali feldspar as an alteration product of glass exhibiting a pronounced peak in abundance. The upper 60-80 m of the Topopah Spring Tuff is a crystal-rich quartz-latite which is composed of 70-80 weight percent alkali feldspar (with average composition $Or_{0.47}Ab_{0.44}An_{0.09}$), with the remaining portion divided between silica polymorphs. In the lower 250–300 m of the Topopah Spring, the abundance of feldspar with average composition $Or_{0.58}Ab_{0.36}An_{0.06}$ is fairly constant at about 55–65 weight percent, with the remaining portion divided between silica polymorphs. A vitrophyre about 10 to 40 m thick is at the base. There is significant heterogeneity in the abundance of individual silica polymorphs over narrow sampling intervals in the Topopah Spring Tuff. The total weight percent silica (tridymite + cristobalite + quartz + opal-CT), however, is relatively constant, at 30 to 40 weight percent in the rhyolitic tuff of the Topopah Spring.

Table 2-5. Hydrostratigraphic units and their depth from the surface and elevation above mean sea level derived from wells USW G-4 and UE-25 UZ #16

Unit	USW G-4 depth (m)	USW G-4 elevation (amsl)	UE-25 UZ#16 depth (m)	UE-25 UZ#16 elevation (amsl)
Alluvial Fill	–	–	0–12.1	1312.7-1300.6
Tiva Canyon Tuff	9.1–45.1	1358.0–1322.0	12.1-49.0	1300.6-1263.7
Yucca Mountain Tuff	45.1–51.3	1322.0–1315.8	–	–
Pah Canyon Tuff	51.3–69.5	1315.8–1297.6	–	–
Paintbrush Bedded Tuffs	–	–	49.0–63.9	1263.7–1248.8
Topopah Spring Tuff (Tpt)	69.5–428.7	1297.6–938.4	63.9–366.2	1248.8–946.5
Calico Hills Formation (Ta)	428.7–519.8	938.4-847.3	366.2-443.6	946.5-869.1
pre-Ta bedded tuffs	519.8–537.3	847.3–829.8	443.6–452.6	869.1–860.1
Prow Pass Tuff	537.3–681.7	829.8–685.4	452.6–513.3*	860.1–799.4
Bullfrog Tuff	681.7–836.1	685.4–531.0	–	–
Tram Tuff	836.1–914.4*	531.0–452.7	–	–
static water level (swl)	541.3	825.8	489.2	823.5
*Total depth: USW G-4 = 914.4 m; UE-25 UZ #16 = 513.3 m				

Total silica polymorph abundance decreases sharply in the quartz latite cap and immediately above and within the basal vitrophyre. Some of the heterogeneity in silica polymorph abundance is due to fracture mineralogy. A thin clay-rich layer forms immediately above the basal vitrophyre, again suggesting preferential flow along the vitrophyre interface.

Below the basal vitrophyre and in the upper part of the Calico Hills Formation, clinoptilolite increases markedly. Clinoptilolite abundance of as much as 80 percent occurs over narrow intervals, with a thickness of 50 m with 55 to 60 weight percent. Clinoptilolite seems to form at the expense of feldspar, with increasing clinoptilolite mirrored by decreases in feldspar abundance. Heterogeneity is pronounced, particularly in the silica polymorphs. In USW G-4, cristobalite (including opal-CT) is the dominant silica polymorph, whereas in UE-25 UZ #16 quartz and opal-CT occur in roughly equal amounts. Total silica polymorph abundance does not vary as much as individual polymorph abundance, and is less than in the devitrified part of the Topopah Spring (about 25 percent versus 35 percent, respectively). Beneath the Calico Hills Formation, the Prow Pass Tuff down to the water table is almost completely quartz and alkali feldspar (about 40 and 55 weight percent, respectively), with minor smectite.

As noted by Johnson and Glassley (1996) the transformation of cristobalite to quartz creates porosity as a result of the larger cristobalite molar volume compared to quartz. However, the volume fraction used for cristobalite seems too high by roughly a factor of two compared to observed mineral abundances (see figure 2-5). This would enhance the change in porosity compared to lower and more reasonable initial cristobalite concentrations. The increase in porosity is proportional to the cristobalite volume fraction as given by the expression

$$\Delta\phi = \phi - \phi_0 = \left(1 - \frac{\bar{V}_{qtz}}{\bar{V}_{cris}}\right) \phi^0_{cris}. \qquad (2\text{-}11)$$

Here ϕ_0 represent the initial porosity before transformation, and ϕ^0_{cris} denotes the initial volume fraction of cristobalite. The quantities $\bar{V}_{qtz}$ = 22.688 cm^3/mole and $\bar{V}_{cris}$ = 25.75 cm^3/mole denote the molar volumes of quartz and alpha-cristobalite, respectively.

2.2.2 Porosity-Permeability

The transformation of cristobalite to quartz and alteration of other silicate minerals may lead to changes in porosity and hence permeability of the YM tuff. Several phenomenological expressions exist for relating porosity and permeability (Oelkers, 1996). One relation is the power law expression

$$\kappa = \kappa_0 \left[\frac{\phi}{\phi_0}\right]^n, \qquad (2\text{-}12)$$

where κ_0 and ϕ_0 refer to the initial permeability and porosity, respectively, and n is a constant. Shown in figure 2-6 is a comparison of the resulting change in permeability for complete alteration of cristobalite to quartz for the initial volume fraction for cristobalite given by Johnson and Glassley (1996) (0.39) and the value taken from figure 2-5 (0.14), plotted as a function of the exponent n.

Robinson (1994) carried out a two-dimensional (2D) calculation using a repository-scale model with a single component, SiO_2, taking into account reaction with quartz. Robinson concluded that the dryout zone could be extended due to precipitation and dissolution of quartz as a result of an increase in permeability. However, the permeability-porosity relation used by Robinson seems highly questionable. He associated a 6 order of magnitude change in permeability with a variation in porosity from 0.09 to 0.13. For the power law representation of permeability on porosity, Eq. (2-12), an exponent of approximately 37.5 would be required to produce this change in permeability. A typical value used in the literature is of the order 3, corresponding to Archie's law (Archie, 1952; Norton and Knapp, 1977). No attempt was made by Robinson to estimate changes in pH and salinity due to evaporation and condensation processes.

MULTIFLO calculations were performed for the repository-scale model (see figure 2-2) with a simplistic representation of the YM host rock consisting of equal amounts of quartz and cristobalite with initial volume fractions set at 0.14, and with an initial porosity of 0.11 as derived from figure 5. Shown in figure 2-7 are the volume fractions for cristobalite and quartz and the porosity depicted as a function of depth for an elapsed time of 1,000 y. As can be seen from the figure, a slight increase in porosity occurs in the vicinity of the repository as cristobalite is transformed into quartz over a depth of several

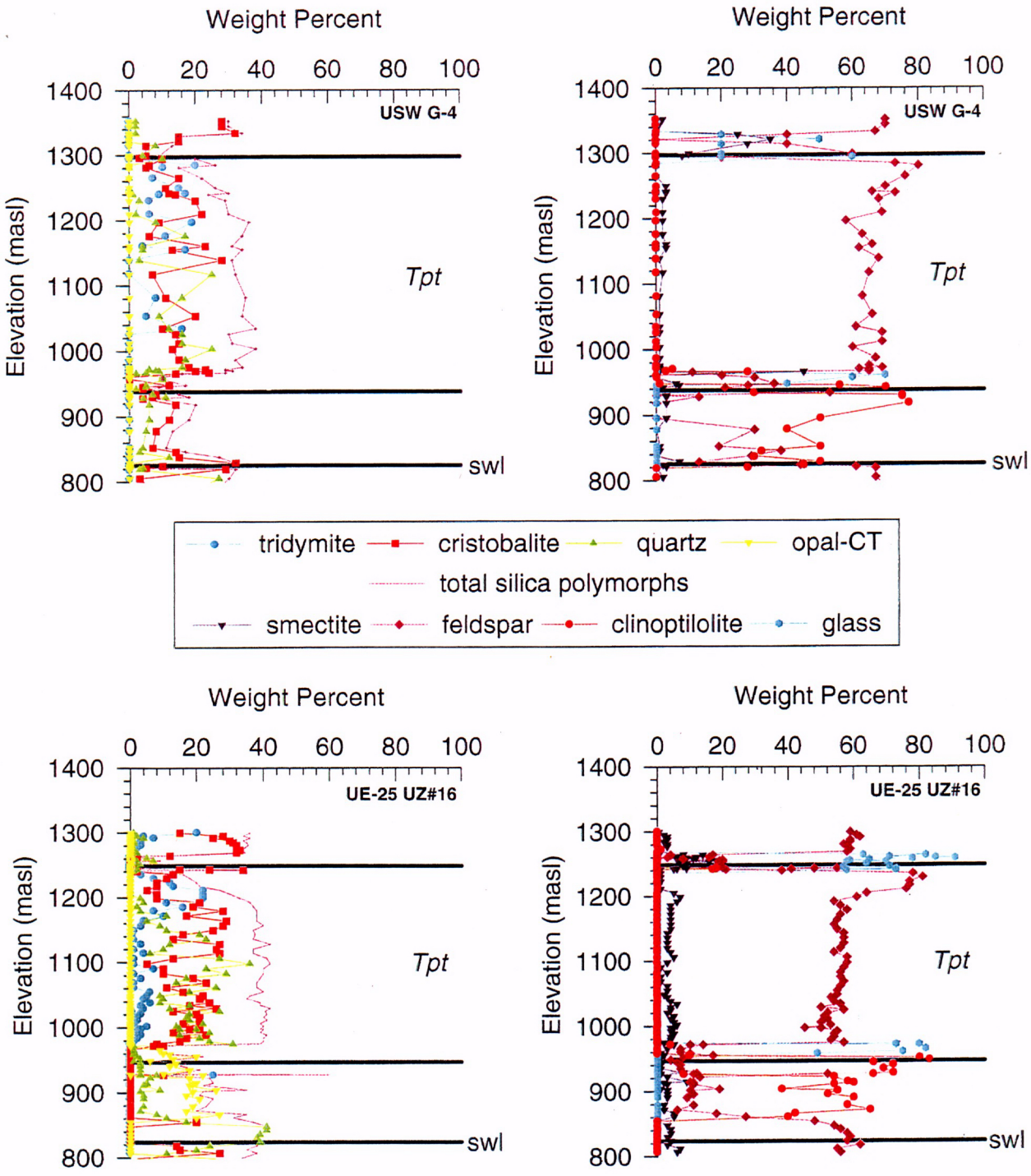

Figure 2-5. Variations in matrix mineralogy with depth (Vaniman et al., 1996)

C-03

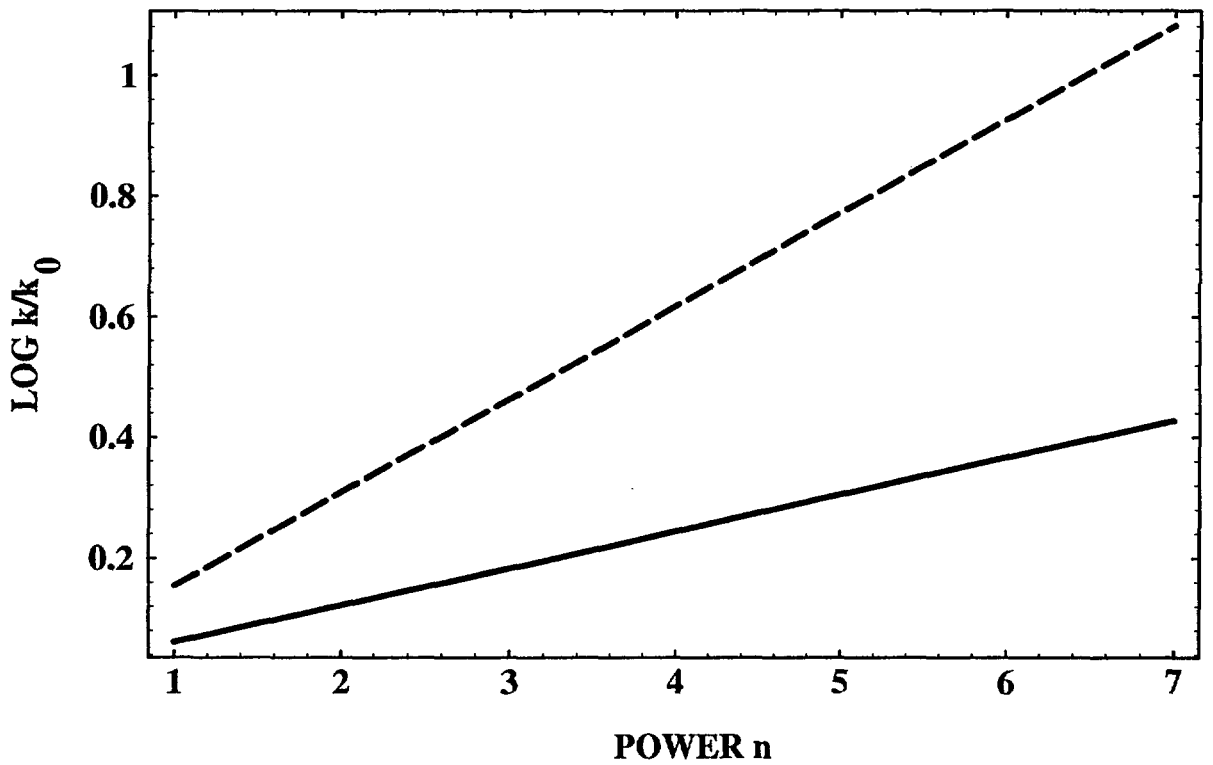

Figure 2-6. Log permeability enhancement factor plotted as a function of the exponent in Eq. (2-12) for the alteration of cristobalite to quartz. The solid line is for an initial cristobalite volume fraction of 0.14, and the dashed line 0.39 used by Johnson and Glassley (1996).

hundred meters. Rate constants for cristobalite and quartz were taken as log$k$ [moles cm^{-2} s^{-1}] = −16.34 and −17.39, respectively, with equal specific surface areas of 10 cm^{-1}. The activation enthalpy was assumed to be the same for both minerals and equal to 75 kJ $mole^{-1}$ (Dove, 1995).

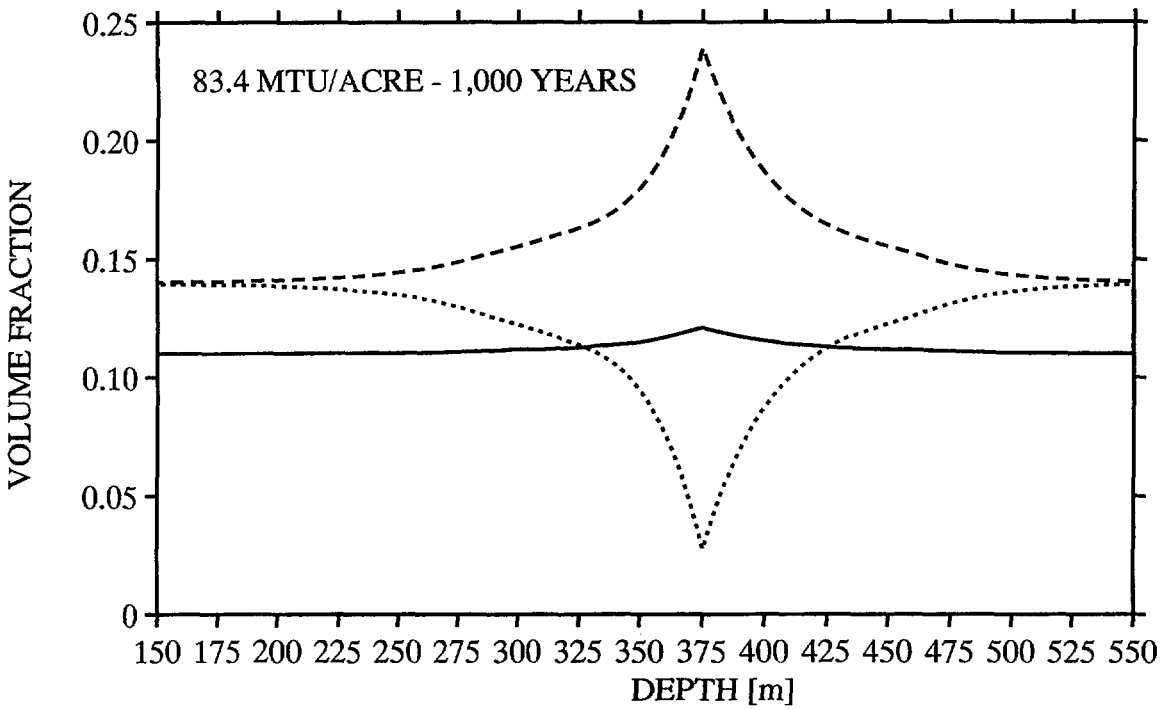

Figure 2-7. Volume fractions for cristobalite (dotted curve) and quartz (dashed curve) depicted as functions of depth for an elapsed time of 1,000 y. Also shown is the porosity (solid curve). Calculations were performed using MULTIFLO based on the repository-scale model (Fig. 2-2).

3 DISCUSSION

There are several important caveats to the MULTIFLO calculations based on the repository-scale model that should be kept in mind. Although the aim of the calculations was to estimate the solution chemistry and rock properties in the near-field, it is in this region where the repository-scale model is least accurate. Because the model represents the HLW as uniformly smeared out over a disk whose radius determines the repository thermal loading, the detailed geometry of the waste package design and waste emplacement is not accounted for in the model. This has important implications on the applicability of the repository-scale model to predicting the near-field environment. For example, temperatures will probably be higher at the drift scale than predicted by the repository-scale model. This would imply reduced liquid saturation, possibly leading to complete dryout very near the drift wall surrounding a waste canister. A probable consequence is increased salinity compared to that predicted by the repository-scale model.

Another important limitation is use of the equivalent continuum model. This model is based on the assumption of capillary equilibrium between fractures and the rock matrix. A restriction which drastically limits the ability of the model to account for simultaneous surficial infiltration and redistribution of moisture produced by heat generated from the waste. An artifact of this model requires that before flow can take place in the fracture, the matrix must first become completely saturated—which is not what is observed at YM. Infiltration is expected to lead to dilution of the aqueous solution composition in the near field, a process which can not be represented in present modeling efforts which are based on the equivalent continuum assumption.

Given these reservations, the repository-scale model should be viewed only as a first attempt to estimate the near-field environment of the repository. However, drift-scale THC models are computationally much more difficult and it may take some time before such calculations are readily available. One key aspect that the repository-scale model may resolve is the role of heat pipes and their associated continuous evaporation and condensation in concentrating the aqueous solution composition in the near field. The results of this ongoing study suggest that concentration of the solution may be far less than expected on the basis of closed system calculations such as EQ6, which neglect the reflux of condensate and its mixing with ambient groundwater.

4 CONCLUSION AND FUTURE WORK

There are several conclusions that may be drawn based on this study.

- Used by itself, EQ6 does not appear capable of predicting changes in aqueous solution composition in the near field. TH calculations for the particular repository loading and geometry are necessary to provide the amount of water evaporated and the rate at which rewetting takes place.

- One of the main problems in applying an uncoupled model such as EQ6 to describe changes in solution composition resulting from evaporation appears to be the difficulty in setting appropriate boundary conditions that represent the situation likely to be found in the near-field environment.

- Altered zone calculations presented by Johnson and Glassley (1996) rely on extreme assumptions of infiltration rates, infiltrating solution composition, mineral reaction rates, temperature etc., which renders their calculations difficult to interpret. The calculations appear to be conceptually flawed in several ways. The main conclusions that "... significant porosity changes will occur in the post-emplacement, repository-block environment." and "Long term performance assessment of this environment must explicitly account for such porosity evolution and its effect on dependent geochemical and hydrologic processes," appear to be inadequately supported.

- To be consistent, whatever limits are set on the solution salinity should also be used when evaluating transport in the near field. This clearly could greatly complicate sorption calculations if the salinity were high, approaching a brine. Consequently, a more accurate estimate of solution composition is preferred.

- Results for pH, calcium, silica and other species are more difficult to estimate without using a fully coupled THC model because of the necessity for additional assumptions about the gas phase, for example. These species potentially affect the formation of secondary minerals, which in turn affect the possible changes in porosity and permeability. Furthermore, neither of the gas-phase boundary conditions used in the EQ6 calculations is likely to occur in the repository.

Future work will consider the case of complete dryout resulting in the formation of salt precipitates. Because dryout occurs much more rapidly than rewetting, it is possible that a prolonged period of increased salinity will result during the rewetting phase as salts redissolve in the presence of small amounts of liquid water. In addition, MULTIFLO calculations need to be performed at the drift scale. Temperatures are higher at the drift scale compared to the repository-scale model, and complete dryout can be expected to occur at lower heat loads. Finally, the effects of infiltration on near-field chemistry and mineral alteration need to be assessed. This will require relaxing the stringent conditions imposed by the equivalent continuum model.

5 REFERENCES

Archie, G. 1952. Introduction to petrophysics of reservoir rocks. *American Association Petrology Geological Bulletin* 34: 943–961.

Buscheck, T.A., and J.J. Nitao. 1993. The analysis of repository-heat-driven hydrothermal flow at Yucca Mountain. *Proceedings of the Fourth Annual International High-Level Radioactive Waste Management Conference.* La Grange, Park IL: American Nuclear Society: 847–867.

Dove, P. 1995. Controls on silica reactivity in weathering environments. In Chemical Weathering Rates of Silicate Minerals, A.F. White and S.L. Brantley eds. *Reviews in Mineralogy* 31: 235–290.

Glassley, W.E. 1996. *Equilibrium bounds on water chemistry and mineralogical changes produced by near-field relative humidity changes.* UCRL-LR-124998. Livermore, CA: Lawrence Livermore National Laboratory.

Harrar, J.E., J.F. Carley, W.F. Isherwood, and E. Raber. 1990. *Report of the Committee to Review the Use of J-13 Well Water in Nevada Nuclear Waste Storage Investigations.* UCID-21867. Livermore, CA: Lawrence Livermore National Laboratory.

Johnson, J.W., and W.E. Glassley. 1996. *Formation of flow and transport barriers without the altered zone.* UCRL-LR-124998. Livermore, CA: Lawrence Livermore National Laboratory.

Lichtner, P.C. 1996. Continuum formulation of multicomponent-multiphase reactive transport. In Reactive Transport in Porous Media. P.C. Lichtner, C.I. Steefel, and E.H. Oelkers, eds. *Reviews in Mineralogy* 34: 1–81.

Lichtner, P.C., and J.C. Walton. 1994. *Near-field liquid-vapor transport in a partially saturated high-level nuclear waste repository.* CNWRA 94-022. San Antonio, Texas: Center for Nuclear Regulatory Analyses.

Lichtner, P.C., and M.S. Seth. 1996a. Multiphase-multicomponent reactive transport nonisothermal reactive transport in partially saturated porous media. *Presented at the International Conference on Deep Geological Disposal of Radioactive Waste, Canadian Nuclear Society.* Winnipeg, Manitoba, Canada.

Lichtner, P.C., and M.S. Seth. 1996b. *User's manual for MULTIFLO: Part II MULTIFLO 1.0 and GEM 1.0, Multicomponent-multiphase reactive transport model.* CNWRA 96-010. San Antonio, TX: Center for Nuclear Regulatory Analyses.

Murphy, W.M., and R.T. Pabalan. 1994. *Geochemical investigations related to the Yucca Mountain environment and potential nuclear waste repository.* NUREG/CR-6288. Washington, DC: U.S. Nuclear Regulatory Commission.

Nitao, J.J. 1996. *Reference Manual for the NUFT Flow and Transport Code, Version 1.0.* UCRL-ID-113520, Livermore, CA: Lawrence Livermore National Laboratory.

Norton, D., and R. Knapp. 1977. Transport phenomena in hydrothermal systems: The nature of porosity. *America Journal of Science* 277: 913–936.

Oelkers, E.H. 1996. Physical and chemical properties of rocks and fluids for chemical mass transport calculations. In Reactive Transport in Porous Media. P.C. Lichtner, C.I. Steefel, and E.H. Oelkers, eds. *Reviews in Mineralogy* 34: 131–191.

Pruess, K. 1991. *TOUGH2—A general purpose numerical simulator for multiphase fluid and heat flow.* LBL-29400. Berkeley, CA: Lawrence Berkeley Laboratory.

Pruess, K., and Y. Tsang. 1994. *Thermal Modeling for a Potential High-Level Nuclear Waste Repository at Yucca Mountain, Nevada.* LBL-35381, UC-600. Berkeley, CA: Lawrence Berkeley Laboratory.

Robinson, B. 1994. *Status of Coupled Thermohydrologic Geochemical Modeling.* DOE-NRC Technical Exchange.

Seth, M.S., and P.C. Lichtner. 1996. *User's manual for MULTIFLO: Part I Metra 1.0 beta, Two-phase nonisothermal flow simulator.* CNWRA 96-005. San Antonio, TX: Center for Nuclear Regulatory Analyses.

Steefel, C.I., and S.B. Yabusaki. 1995. *OS3D/GIMRT: Software for modeling multicomponent-multidimensional reactive transport.* User's manual and programmer's guide, Version 1.0, 58 p.

van Genuchten, M. 1980. A closed form equation for predicting the hydraulic conductivity of unsaturated soils. *Soil Science Society of American Journal* 44: 892–898.

Vaniman, D.T., D.L. Bish, S.J. Chipera, B.A. Carlos, and G.D. Guthrie. 1996. *Summary and Synthesis Report on Mineralogy and Petrology Studies for the Yucca Mountain Site Characterization Project.* Volume 1. Chemistry and Mineralogy of the Transport Environment at Yucca Mountain. Milestone 3665. U.S. Department of Energy. Earth and Environmental Sciences. Los Alamos, NM: Los Alamos National Laboratory.

Walton, J.C. 1993. Effects of evaporation and solute concentration on presence and composition of water in and around the waste package at Yucca Mountain. *Waste Management* 13: 293–301.

White, S.P. 1995. Multiphase nonisothermal transport of systems of reacting chemicals. *Water Resource Research.* 31: 1,761–1,772.

Wilder, D.G. 1996. Editor Volume II: *Near-field and altered-zone environment report.* UCRL-LR-124998. Livermore, CA: Lawrence Livermore National Laboratory.

Wolery, T.W. 1992. *EQ3/6, a software package for geochemical modeling of aqueous systems. Package overview and installation guide (Version 7.0).* UCRL-MA-110662. Livermore, CA: Lawrence Livermore National Laboratory

Zyvoloski, G., Z. Dash, and, S. Kelkar. 1992. FEHMN 1.0: *Finite element heat and mass transfer code.* LA-12062-MS, Rev 1. Los Alamos, NM: Los Alamos National Laboratory.

APPENDIX

MINERAL REACTION RATES

MINERAL REACTION RATES

The kinetic rate law for minerals is usually based on transition state theory. The expression for the reaction rate has the form (Aagaard and Helgeson, 1982)

$$I_m = -k_m s_m (1-K_m Q_m), \tag{A-1}$$

where k_m denotes the kinetic rate constant, s_m represents the reactive mineral surface area, K_m refers to the equilibrium constant for the reaction, again a function of temperature and pressure, and Q_m denotes the ion activity product. Thus for the reaction

$$\sum_{j=1}^{N_c} \nu_{jm} A_j \rightleftharpoons M_m, \tag{A-2}$$

the ion activity product is defined as

$$Q_m = \prod_{j=1}^{N_c} (\gamma_j C_j)^{\nu_{jm}}, \tag{A-3}$$

with concentration C_j and activity coefficient γ_j,

A.1. Rate Constants

The rate constant may be a function of temperature, pressure and various solution variables such as pH and therefore is not really a constant (Oelkers et al., 1994). The reaction rate constant may be expressed in units of moles cm^{-2} s^{-1} (k_m) or vol. % s^{-1} (K'_m):

$$k'_m = 100 \times \bar{V}_m k_m, \tag{A-4}$$

with molar volume $\bar{V}_m$. The pH dependence of the rate constant typically enters as a power law of the form

$$k_m = a_{H^+}^n k_m^\circ, \tag{A-5}$$

where k_m° is independent of pH. The power n may be positive or negative. A more general form for the pH-dependent rate constant is given by

$$k_m = k_m^0 + k_m^a a_{H^+}^{n_m^a} + k_m^b a_{H^+}^{n_m^b}. \quad \text{(A-6)}$$

Here k_m^a and k_m^b refer to the acidic and basic pH regions, respectively, and k_m^0 refers to the neutral pH region. For albite (Blum and Stillings, 1995), $logk_m{}^0 = -16$, $\log k_m{}^a = -13.875$, $\log k_m{}^b = -18.472$, $n_m{}^a = 0.5$, and $n_m{}^b = -3$.

A.2 Surface Area

One of the most difficult and problematic physical properties to determine is the surface area of the reacting minerals. This parameter occurs as a multiplicative factor in the rate expression. An effective rate constant may be defined as the product of the rate constant at a given temperature times the surface area. The uncertainty in the effective rate constant reflects uncertainty in both the rate constant and mineral surface area. For a sufficiently large effective rate constant, the actual reaction becomes transport controlled; in this regime the reaction rate is largely insensitive to the rate constant or surface area. However, for surface controlled reactions and short time spans (Murphy et al., 1989; Lichtner, 1993), the rate constant and surface area become important factors in determining the reaction rate. Mineral surface area may be expressed in a variety of ways depending on the reference volume chosen. The relationship between the surface areas expressed relative to a representative elemental volume (REV) and volume of fluid is given by

$$\alpha_V = \phi \rho_f \alpha_f, \quad \text{(A-7)}$$

where α_v refers to the REV volume-based surface area, α_f refers to the surface area based on a volume of fluid (usually taken as 1 kg H_2O), ρ_f denotes the fluid density in the appropriate units [kg cm^{-3}], and ϕ denotes the porosity. Grain size b_m mineral concentration, and surface area can be related using the phenomenological relationship

$$\alpha_m = \frac{6}{b_m} \phi_m. \quad \text{(A-8)}$$

This equation is based on a simple geometric model of cubical or spherical grains surrounded by an aqueous solution.

A.3. Temperature Variation of Kinetic Rate Constant

The kinetic rate constant is assumed to vary with temperature according to an Arrhenius-type equation (Helgeson et al., 1984)

$$k_m(T) = k_m^0 \frac{T}{T_0} \exp\left[-\frac{1}{R}\left(\frac{1}{T}-\frac{1}{T_0}\right)\Delta H_m^\dagger\right], \quad \text{(A-9)}$$

where k_m^0 denotes the rate constant at the reference temperature T_0 and $\Delta H_m^\dagger$ denotes the activation enthalpy.

A.4 Time for Complete Dissolution

For far-from-equilibrium conditions the mineral mass transfer equation reduces to

$$\frac{\partial \phi_m}{\partial t} = -\bar{V}_m \, k_m \, \alpha_m, \tag{A-10}$$

where ϕ_m denotes the volume fraction of the mth mineral with molar volume $\bar{V}_m$. In general, the surface area varies with reaction. A simple phenomenological relation is based on a power law equation of the form

$$\alpha_m = \alpha_m^0 \left[\frac{\phi_m}{\phi_m^0}\right]^\sigma, \tag{A-11}$$

where σ is a constant $(0 \; \sigma < 1)$, and s_m^0 and ϕ_m^0 denote the initial surface area and volume fraction, respectively. With this expression for the surface area, the differential equation for the mineral volume fraction may be integrated to give

$$\left[\frac{\phi_m(t)}{\phi_m^0}\right]^{1-\sigma} = 1-(1-\sigma) \; \tau_m, \tag{A-12}$$

where

$$\tau_m = \frac{\phi_m^0}{\bar{V}_m k_m \alpha_m^0}. \tag{A-13}$$

Thus, the time required for the mineral to completely dissolve $\left[\left(\phi_m \; (t) = 0\right)\right]$ is given by

$$t_{diss} = \frac{\tau_m}{1-\sigma}. \tag{A-14}$$

For σ = 2/3 relating volume to surface area, it follows that

$$t_{diss} = 3\tau_m. \tag{A-15}$$

The value of t_{diss} is tabulated in table 2-4 for primary minerals assuming an initial volume fraction of 0.1. However, this formulation does not provide for the possibility of an increase in surface area with dissolution as might occur due to the formation of etch pits, for example. In a partially saturated medium, the reacting mineral surface is proportional to the wetted surface area. Here it is assumed that the pore surface is completely wetted by the aqueous solution for saturations above the residual saturation, the threshold for Darcy flow of liquid.

REFERENCES

Aagaard P., and H.C. Helgeson. 1982. Thermodynamic and kinetic constraints on reaction rates among minerals and aqueous solutions. I. Theoretical considerations. *American Journal of Science* 282: 237–285.

Blum, A.E., and L.L. Stillings. 1995. Feldspar dissolution kinetics. In Chemical Weathering Rates of Silicate Minerals. A.F. White and S.L. eds. *Reviews in Mineralogy* 31: 291–342.

Helgeson, H.C., W.M. Murphy, and P. Aagaard. 1984. Thermodynamic and kinetic constraints on reaction rates among minerals and aqueous solutions. II. Rate constants, effective surface area, and the hydrolysis of feldspar. *Geochimica et Cosmochimica Acta* 51: 3,137–3,153.

Lichtner, P.C. 1993. Scaling properties of kinetic mass transport equations. *American Journal of Science* 293: 257–296.

Murphy, W.M., E.H. Oelkers, and P.C. Lichtner. 1989. Surface reaction versus diffusion control of mineral dissolution and growth rates in geochemical processes. *Chemical Geology* 78: 357–380.

Oelkers, E.H., J. Schott, and J.L. Devidal. 1994. The effect of aluminum, pH, and chemical affinity on the rates of aluminosilicate dissolution reactions. *Geochimica et Cosmochimica Acta* 58: 2,011–2024.